Chaotic electron dynamics in antidot lattice subjected to strong in-plane magnetic field

N. M. Sotomayor Choque, G. M. Gusev, and J. R. Leite
Instituto de Física da Universidade de São Paulo, Caixa Postal 66318, CEP 05315-970, São Paulo, Brazil

A. A. Bykov, L. V. Litvin, N. T. Moshegov, and A. I. Toropov
Institute of Semiconductor Physics, Novosibirsk, Russia

D. K. Maude
GHMFL, MPI-FKF/CNRS, BP-166, F-38042, Grenoble, Cedex 9, France

J. C. Portal
GHMFL, MPI-FKF/CNRS, BP-166, F-38042, Grenoble, Cedex 9, France;
INSA-Toulouse, 31077, Cedex 4, France;
and Institut Universitaire de France, Toulouse, France

(Received 22 January 2002; revised manuscript received 11 March 2002; published 23 July 2002)

The classical electron dynamics in two-dimensional antidot lattices subjected to a magnetic field with a strong in-plane component is studied numerically. The anisotropy of the Fermi contour of the two-dimensional electron gas, produced by the parallel field, strongly modify the electron trajectories. We calculate the Poincaré surface of the section, and magnetoresistance with such distorted Fermi contour and obtain good agreement with experimental results.

DOI: 10.1103/PhysRevB.66.035324 PACS number(s): 81.40.Rs, 72.10.−d, 72.20.−i, 72.15.−v

I. INTRODUCTION

During the past decade the antidots arrays in semiconductor heterostructures, which contain the two-dimensional electron gas (2DEG), was a model system that allowed to study the chaotic classical dynamics in condensed-matter physics.[1–6] This system has been considered as an experimental realization of the theoretical model of the billiard of Sinai.[7] The chaotic dynamics of the 2DEG in antidot lattices with different pattern shape and periodicity configuration has been studied principally in the presence of magnetic field directed perpendicularly to the surface of the samples.[2,8–14]

The motion of electrons has also been investigated in phase space by means of Poincaré surface of sections.[11,12,15] In these maps periodical and quasiperiodical orbits can be identified as islands, in phase space, surrounded by a chaotic sea. Regular electron orbits lead to anomalous peaks in the magnetoresistance, which are the so-called commensurability peaks. In square antidot lattices last maximum appears in resistivity when the cyclotron diameter, $2R_c$, is equal to the period of the array a. Depending on the array geometry these maxima have been attributed to the existence of pinned orbits around groups of antidots,[3,16] or runaway trajectories skipping regularly from one antidot to another.[12,17,18] Fleischmann, Geisel, and Ketzmerick,[15] through theoretical calculations, demonstrated that the commensurability oscillations are mainly produced by the correlation function of unperturbed chaotic motion that reflected the presence of nonlinear resonances. According to this theory chaotic trajectories trapped temporarily in the vicinity of regular islands, at commensurate values of B, are responsible for the main contribution for the magnetoresistance ρ_{xx} peaks.[6] Regular orbits also strongly depend on the shape of the antidots, in this way, in elliptically shaped antidots magnetorsistance peaks have been attributed to regular trajectories colliding ballistically with a single antidot.[19] In cross-shaped antidot lattices several types of regular trajectories, simultaneously trapped in the potential minimum between four crosses, can be responsible for main maximum in the magnetoresistance.[20] Because the dynamics of the 2DEG in antidot lattice is extremely sensitive, to external parameters, it is also possible to check the influence of internal parameters such as electron energy and dispersion on the particle trajectories.

Recently it has been predicted that the Fermi contour of the 2DEG, which is originally isotropic, can be distorted by the in-plane magnetic field.[21,22] Therefore a technique utilizing 2D array of antidots could, in principle, be used to determine the anisotropy of the Fermi contour of the 2D electron gas subject to in-plane magnetic field. This distortion of the Fermi surface in the 2DEG has been studied by cyclotron resonance in the infrared region of the optical spectra,[23] temperature damping of Shubnikov-de Haas oscillations,[24] and magnetic electron focusing effect.[25] It has been shown that the asymmetry of the confinement potential of the 2DEG, combined with the tilted magnetic field, lead to the egglike Fermi contour due to an increase of the electron effective mass.[26] In the quasiclassical picture the electrons move along real-space trajectories with orbit shapes that are similar to the shape of the Fermi contour, therefore, it could be expected that the chaotic dynamics of 2D electrons in antidot lattice under tilted magnetic field will be modified.

In this paper, we present, the results of our study on the evolution of the electron dynamics in antidots arrays, in a two-dimensional system, when subjected to an increasing in-plane magnetic field. Through the analysis of the calculated Poincaré surfaces of the section, for different values of the parallel component of the field, we found a strong transfor-

mation of the electron dynamics, and evolution of the commensurability peaks of the longitudinal resistivity ρ_{xx}. Several regular trajectories, which are not observed in perpendicular magnetic field, appear and lead to enhancement of diffusion in the longitudinal direction. We compare our calculatations with experimental magnetotransport data obtained for antidots arrays, with different lattice periods, in high mobility GaAs/Al_xGa_{1-x}As samples.

The samples were subjected to increasing in-plane magnetic field up to 28 T, this produces a shift of the magnetoresistance commensurability peaks toward higher values of the magnetic field, and also a strong broadening as the in-plane component of the field increases. Also, we observed a commensurability peak, corresponding to the condition $R_c = a$, for the sample with the shortest period, in presence of almost parallel magnetic field. We attribute all these phenomena to the distortion of the Fermi contour in the two-dimensional electron gas subject to in-plane magnetic field.

The paper is organized as follows, in Sec. II A we briefly outline a description of the electronic structure of the 2DEG in the presence of tilted magnetic field. In Sec. II B we describe the analytical model employed to simulate the electron dynamics in antidot lattices in the presence of perpendicular magnetic field. In Sec. II C, we explain the analytical approximation developed to simulate the electron motion in 2D antidot lattice subjected to tilted magnetic field. In Sec. III we discuss the results for the calculated Poincaré surface of sections in perpendicular and tilted magnetic field and also of the evolution of the calculated magnetoresistance commensurability peaks in the presence of increasing parallel magnetic field. In Sec. IV A we present a description of the samples fabricated for this work and also of the experimental setup employed. In Sec. IV B we show the results of our experimental magnetotransport measurements and make a discussion of the results comparing them with those obtained by simulations.

II. THEORETICAL MODEL FOR ANTIDOT ARRAYS SUBJECT TO IN-PLANE MAGNETIC FIELD

A. Electronic structure in parallel magnetic field

We consider GaAs/Al_xGa_{1-x}As heterostructures confining a 2DEG to a plane perpendicular to the z axis. If the magnetic field $B = B_x$ lies along the x direction, the Hamiltonian of an electron confined to the x-y plane by a potential $V_c(z)$ is found to be

$$H = \frac{1}{2m^*}(\vec{p} + q\vec{A})^2 + V_c(z), \tag{1}$$

where m^* is the electron effective mass, $\vec{p}$ is the momentum operator, q is the carrier charge, and $\vec{A}$ is the potential vector chosen to be of the form

$$\vec{A} = (0, -B_x z, 0). \tag{2}$$

In an explicit way the whole Hamiltonian is written as

$$H = \frac{1}{2m^*}(p_y - eB_x z)^2 + \frac{p_x^2}{2m^*} + \frac{p_z^2}{2m^*} + V_c(z). \tag{3}$$

The energy spectrum is formed by subbands and the eigenenergies $E_n(k_x, k_y)$, $n = 0,1\ldots$ are functions of the quasicontinuous wave vectors k_x and k_y. For the particular case of a parabolic potential $V_c(z) = \frac{1}{2}m^*\Omega^2 z^2$, the eigenenergies can be found, explicitly, in analytic form[22]

$$E_n(p_x, p_y) = \left(n + \frac{1}{2}\right)\hbar\tilde{\omega} + \frac{1}{2m^*}p_x^2 + \frac{1}{2m_y^*}p_y^2, \tag{4}$$

where $n = 0,1,\ldots$, $\tilde{\omega} = (\omega_x^2 + \Omega^2)^{1/2}$, $\omega_x = |e|B_x/m^*$, and $m_y^* = m^*\tilde{\omega}^2/\Omega^2$, is the induced effective mass for the y component of the electron motion, which grows with B_x.

For the particular case of our samples we have only the lowest energy subband occupied, so in Eq. (4), $n = 0$. We see, that the in-plane magnetic field influences the electron motion in z and y directions and does not change the motion in x direction. In z direction the eigenenergy of the harmonic oscillator in zero field $\frac{1}{2}\hbar\Omega$ is changed to $\frac{1}{2}\hbar\tilde{\omega}$. In the x-y plane the parallel magnetic field induces the new effective mass m_y^* for the y component of the electron motion. Therefore the Fermi contour is distorted from circular shape to an elliptical shape due to an increase of the cyclotron effective mass in comparison with the originally circular shape, the reason is that the cyclotron mass is determined in quasiclassical approximation by the Fermi area A_F surrounded by the Fermi contour $m_c = (\hbar^2/2\pi)(dA_F/dE)$. Corresponding electron trajectories in parallel magnetic field should have elliptical shape too. However, in realistic GaAs/Al_xGa_{1-x}As heterostructures the confining potential is not harmonic, and the energy spectrum must be obtained through self-consistent calculations.[22,27]

The case of the energy spectrum of a two-dimensional electron gas, in semiconductor inversion layers, when the magnetic field is exactly parallel to the spatial-charge layer, has been treated analytically in Ref. 28, where specific expressions for the resulting hybrid electric-magnetic subbands were obtained. The triangular-well approximation of the electrostatic potential $U = F_s z$, where F_s is the surface electric field, was introduced together with the conditions: $\vec{F}_s \| \vec{z}$ and $\vec{B} \| \vec{x}$. Departing from Eqs. (1) and (2), and by introduction of the ansatz $\Psi(x,y,z) = D(z)\exp(ik_x x + ik_y y)$, the energy eigenvalues were found to be

$$\frac{E}{\hbar\omega_c} = \frac{k_x^2 l_B^2}{2} - \frac{k_D^2 l_B^2}{2} + \left(\nu_i + \frac{1}{2}\right) + (k_D l_B)(k_y l_B), \tag{5}$$

where $D(z)$ accounts for the motion along z direction and k_x, and k_y are the wave vectors along x and y directions, respectively, $z_0 = l_B^2(k_y - k_D)$ is the center of coordinates of motion, $l_B = (\hbar/eB)^{1/2}$, is the cyclotron radius, $k_D = mF/\hbar B$ is the wave vector of the drift velocity, ν_i is an index, which in general case, is a function of the center coordinate z_0/l_B and subband index i, $\hbar$ is the reduced Planck constant, and ω_c is the cyclotron frequency.

The parameter $k_D l_B$ is introduced as a measure of the ratio of the electrostatic energy $eF_s l_B$ to the cyclotron energy $\hbar\omega_c$. This parameter can also be expressed as function of the characteristic lengths:

$$k_D l_B = \frac{eF_s l_B}{\hbar\omega_c} = \frac{1}{2}\left(\frac{l_B}{L}\right)^3, \tag{6}$$

where $L=(\hbar^2/2m^* eF_s)^{1/3}$ is the average width of the 2D electron layer.

As in our samples we have only one electric occupied subband the energy spectrum can be considered only for ground hybrid subband and $i=0$. When $k_D l_B \gg +1$ electric quantization is the predominant effect, and magnetic field leads to the small anisotropy and diamagnetic shift of the spectrum, in the magnetic limit, defined as $k_D l_B \ll +1$, when the magnetic energy is much larger than the electrostatic energy, or in other words, the thickness of the 2D layer is larger than the magnetic length, the energy spectrum becomes strongly anisotropic and Fermi contour has an egg shape. A rough estimation of the parameter $k_D l_B$ for realistic GaAs heterostructures is obtained from the values $L=41$ Å, and $l_B=49$ Å at $B=28$ T, which gives $k_D l_B=0.8$. This means that the electrostatic and magnetic quantization are equally important in our samples at $B=28$ T. The magnetic limit condition $k_D l_B \ll +1$ can be estimated approximately by $k_D l_B=0.1$ that can be reached, only, for applied magnetic field of the order $B=112$ T that is larger than we used in our experiments. From this argument we can conclude that the application of a parallel magnetic fields up to 28 T, in the x direction, cannot lead to the fully quantization of the y and z components of momentum, therefore the motion in x-y plane remains continuous, the Fermi contour is fairly anisotropic, and it is still possible to treat the electron dynamics classically.

Self-consistent calculations confirm the existence of the significant differences between results for the parabolic confining potential and realistic potentials for $GaAs/Al_xGa_{1-x}As$ heterojunctions,[26] however, elliptical-like and oval-like trajectories should lead to completely different chaotic dynamics in two-dimensional electron billiard systems. For the simulations of the classical electron dynamics in our samples we have used the self-consistent results obtained in Ref. 27, for the Fermi contour, of similar $GaAs/Al_xGa_{1-x}As$ heterostructures.

B. Model for electron dynamics in antidot arrays

In the following we will consider the classical approximation for the dynamics of an electron in a two-dimensional (2D) potential $U_{2D}(x,y)$ and in perpendicular magnetic field $\vec{B}=(0,0,B_z)$. The Hamiltonian of an electron confined to the x-y plane by a potential $V_{2D}(x,y)$ is found to be

$$H=\frac{1}{2m^*}(\vec{p}-e\vec{A})^2+U_{2D}(x,y), \tag{7}$$

where the potential vector is written as

$$\vec{A}=\left(-\frac{By}{2},\frac{Bx}{2},0\right). \tag{8}$$

Following the approximation proposed by Fleishmann and co-workers,[15] the antidot potential is modelated by the expression

$$U_{2D}(x,y)=U_0\left[\cos\left(\frac{\pi x}{a}\right)\cos\left(\frac{\pi y}{a}\right)\right]^{\beta}, \tag{9}$$

where β controls the stepness of antidots, U_0 defines the strength of the antidot potential, and a represents the period of the antidot lattice. Using a soft-wall approximation we choose $\beta=6\rightarrow 8$ for the lattice with period $a=0.5\rightarrow 1.0$ μm and $\beta=10\rightarrow 12$ for $a=1.5\rightarrow 2$ μm. In order to avoid computational difficulties in calculating the electron dynamics we use dimensionless variables:

$$\tilde{H}=\frac{H}{E_F},\quad \tilde{U}=\frac{U}{E_F},\quad \tilde{x}=\frac{x}{a},\quad \tilde{y}=\frac{y}{a},\quad \tilde{t}=\frac{t}{\tau_0}, \tag{10}$$

where E_F is the Fermi energy.

As a unit to scale time, we use τ_0

$$\tau_0=\left(\frac{m^* a^2}{2E_F}\right)^{1/2}, \tag{11}$$

which corresponds to the time that an electron delay in traveling a distance a at the Fermi speed. The magnetic field was scaled by

$$B_0=\frac{2(2m^* E_F)^{1/2}}{ea}, \tag{12}$$

where $B=B_0$ corresponds to a cyclotron radius of half the length of the period a of the artificial lattice. The equations of motion, omitting tildes, are given by

$$\dot{x}=2\left(p_x+\frac{B}{B_0}y\right), \tag{13}$$

$$\dot{y}=2\left(p_y-\frac{B}{B_0}x\right), \tag{14}$$

$$\dot{p}_x=\frac{B}{B_0}\dot{y}-\frac{\partial U}{\partial x}, \tag{15}$$

$$\dot{p}_y=-\frac{B}{B_0}\dot{x}-\frac{\partial U}{\partial y}. \tag{16}$$

The numerical integration of these equations of motion allows us to study the electron trajectories in phase space by means of the Poincaré surfaces of sections. In order to calculate the magnetoresistance we used classical linear-response theory, because the 2DEG in antidot lattices is essentially a conservative system where the application of a small external electric field produces a heating, which is a quadratic term in the electric field avoiding, eventually, steady-state currents to form.[7] In this way the Ohmic conductivity σ_{ij} is proportional to the diffusivity and is given, by the expression[29]

$$\sigma_{ij}=\frac{N_s e^2}{E_F}\int_0^\infty \langle v_i(t)v_j(t=0)\rangle_\Gamma e^{-t/\tau}dt, \tag{17}$$

where N_s is the electron concentration, E_F is the Fermi energy, $\langle v_i(t)v_j(0)\rangle_\Gamma$ is the velocity-velocity correlation function double averaged over phase space Γ, the indices *i* and *j* stand for the *x* and *y* direction, respectively. The presence of impurity scattering is included through the electron mean scattering time τ, where the probability of an electron not suffering a collision within the time interval [0,t] is given by $e^{-t/\tau}$.

From the numerical computation of the conductivity tensors σ_{xx} and σ_{xy}, as a function of the perpendicular magnetic field, we are able to determine the longitudinal ρ_{xx} and transverse ρ_{xy} resistivities through the expressions

$$\rho_{xx}=\frac{\sigma_{xx}}{\sigma_{xx}^2+\sigma_{xy}^2}, \tag{18}$$

$$\rho_{xy}=\frac{\sigma_{xy}}{\sigma_{xx}^2+\sigma_{xy}^2}. \tag{19}$$

In order to calculate conductivity, we generate an ensemble of electron trajectories, uniformly distributed inside a square region of one period side (distribution of starting points in the unit cell), which encircles the antidot located at the origin of coordinates. From each point of this region we started 5000 electron orbits generated by random initial conditions (angular distribution around each start point).

C. Model for the electron dynamics in antidot arrays with tilted magnetic field

In order to take account of the effects of parallel magnetic field, on the dynamics of the 2DEG, we avoid the difficulties of self-consistent calculation, and instead, we introduce the effects of the Fermi contour distortion as a systematic variation of the electron effective mass in the *x* and *y* directions. This is done in order to preserve the area of the Fermi surface. In this way Eq. (7) can be written, using the same gauge as in Eq. (8) by

$$\frac{1}{2m_x^*}\left\{p_x+\frac{eBy}{2}\right\}^2+\frac{1}{2m_y^*}\left\{p_y-\frac{eBx}{2}\right\}^2+U_{2D}(x,y), \tag{20}$$

where m_x^* and m_y^* are the components of the effective-mass tensor in the *x* and *y* directions. The Fermi energy will be given by

$$\frac{1}{2}m^*\{\alpha V_{Fx}^2+\beta V_{Fy}^2\}, \tag{21}$$

where α and β are two parameters that we introduce in order to fit the data of Ref. 22 for the Fermi circle, V_{Fx} and V_{Fy} are the components of the Fermi velocity along the *x* and *y* directions, respectively. By using the same substitutions as in Eq. (10), the Hamiltonian for this case reads

$$\frac{1}{\alpha}\left\{\alpha\frac{dx}{dt}+\frac{B}{B_0}y\right\}^2+\frac{1}{\beta}\left\{\beta\frac{dy}{dt}-\frac{B}{B_0}x\right\}^2+U_{2D}(x,y). \tag{22}$$

Equation (22) will produce a elliptical Fermi contour for the 2DEG, in order to account for the proper ''egglike'' shape we have added, to this equation, a perturbation term γ of the kind

$$\gamma=\eta\frac{1}{\alpha}\left\{\alpha\frac{dx}{dt}+\frac{B}{B_0}y\right\}^4, \tag{23}$$

where η, is also a parameter, chosen to be small enough and applied only for positive, predetermined, values of $\dot{x}$. The introduction of this term together with the parameters α and β, allows to fit the extrapolated data of Ref. 21 for the proper egglike Fermi contour. In this way the equations of motion read

$$\dot{x}=\left(\alpha p_x+\frac{B}{B_0}y\right)+\gamma, \tag{24}$$

$$\dot{y}=2\left(\beta p_y-\frac{B}{B_0}x\right), \tag{25}$$

$$\dot{p}_x=\frac{B}{B_0\beta}\dot{y}-\frac{\partial U}{\partial x}, \tag{26}$$

$$\dot{p}_y=-\frac{B}{B_0\alpha}\dot{x}-\frac{\partial U}{\partial y}. \tag{27}$$

The integration of this system of equations, generated by a proper egglike Fermi contour coherent with the subband profiles obtained by self-consistent calculations, allows us to obtain the magnetoresistance of the antidot system in 2DEG in the presence of almost parallel magnetic field. Figure 1 shows four curves of the Fermi velocity, in real space, for two-dimensional electrons in the presence of increasing parallel magnetic field from 0 T up to 28 T, these curves were obtained with the approximation described above.

III. DISCUSSION OF THE RESULTS

A. Poincaré surfaces

Following the models for the electron dynamics in perpendicular magnetic field and our approximation for tilted field, we first, calculate the Poincaré maps for the particular case of an antidot diameter at the Fermi energy of $d=0.23a$, which approximately corresponds to the experimental case of our sample with $a=0.5$ μm. A Poincaré surface of section at $y=y_0$ is the intersection of the energy surface with the plane $y=y_0$. Figure 2 shows three Poincaré surfaces of the section at $[y(\mathrm{mod}1)=0]$ for $B/B_0=1$ in the smooth potential generated for 30 randomly chosen initial conditions. In the upper part, marked with (a), we have the case of a surface of the section for perpendicular magnetic field. It is possible to observe several islands around $x=0.5$ surrounded by a chaotic sea. The islands correspond to regular motion

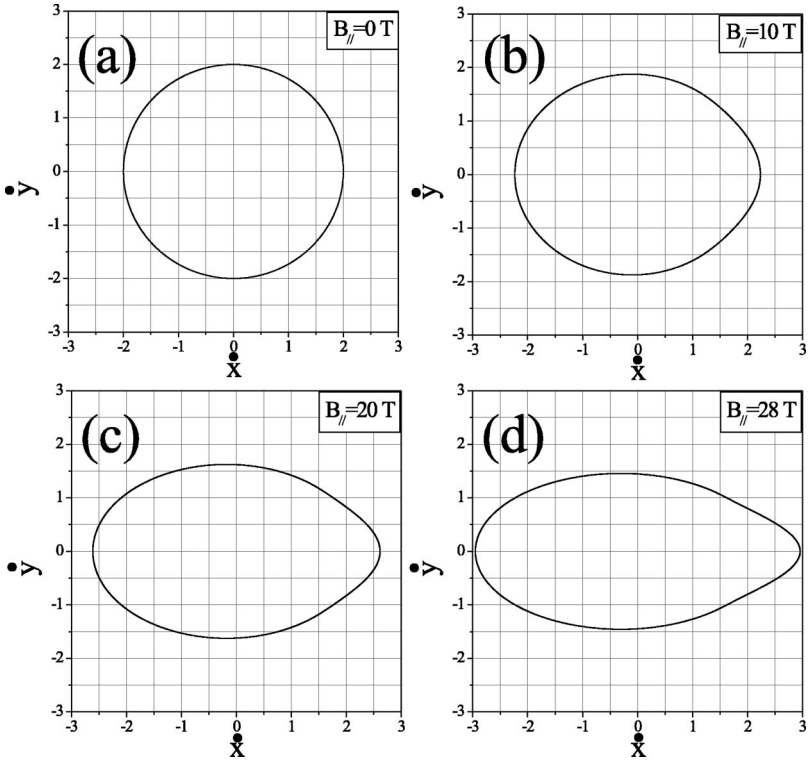

FIG. 1. (a) Real-space velocity, at the normalized Fermi energy, for the 2DEG in perpendicular magnetic field, (b), (c), and (d) show the distortion produced in the Fermi velocity by effect of increasing parallel magnetic field ($B_{\|}=10$ T, 20 T, and 28 T).

and, according to the Kolmogorov-Arnold-Moser theorem,[30] represent the intersections of invariant tori for cyclotronic orbits with $(R_c=a/2)$ revolving around the single antidot located at $(x,y)=(0,0)$. These kind of orbits are known as rosettelike and can be periodic or quasiperiodic.[15] The second figure, marked (b), corresponds to a surface of the section, at $[y(\mathrm{mod}1)=0]$, with the same initial conditions as the previous figure, this time we have a parallel magnetic-field component $B_{\|}$ of 10 T applied on the electron gas. It is possible to observe a severe transformation of the electron dynamics when the in-plane magnetic field is applied. Because of the distortion of the shape of the cyclotron orbits there is an increment on the degree of chaos of the system and, due to this effect, most of the islands of regular motion disappear. The lower figure (c) illustrates the Poincaré surface of the section, at $[y(\mathrm{mod}1)=0]$, with the same conditions as the two previous, this time when a magnetic field with a parallel component of 20 T is applied on the 2DEG. This strong field highly distorts the electron trajectories in the x and y directions due to the elliptical shape of the Fermi line, producing an enhancement of chaos in phase space. Most of the regular islands completely disappear and instead there are several closed loops with different shapes belonging to some invariant tori whose intersections with $[y(\mathrm{mod}1)=0]$ are shown on the left part of the figure. We are also able to observe an increment of drifting trajectories that appear in the surface of section as nonclosed curves or as islands surrounded by a self-similar hierarchy of cantori.[7,31] The effect of shrinking of the area corresponding to stable motion is due to the increase of the cyclotron diameter on the x direction, as the commensurability condition $2R_c=a$ is lost some regular orbits will inevitably change to chaotic due to backscattering with neighboring antidots. These two effects: the increasing of the number of drifting trajectories, and the enhancement of chaos in phase space can be responsible for the broadening of the commensurability peaks when the 2DEG is in the presence of parallel magnetic field.

Due to the anisotropy of the Fermi contour in the x and y direction it is also necessary to look at the electron dynamics in the y direction, so in Fig. 3 we have plotted three Poincaré surfaces of the section at $[x(\mathrm{mod}1)=0]$ for $B/B_0=1$ for the same antidot diameter at the Fermi energy, that in the previous figure. In Fig. 3(a) we will see again the surface of the section for the 2DEG in perpendicular magnetic field. When we compare with Fig. 2(a) with Fig. 3(a) we find no significative differences, between these two maps, because of the isotropy of diffusion along longitudinal and transverse directions. In part (b) and (c) we observe again an increase of the degree of chaos in the system, when the parallel component of the field is applied, some regular trajectories disappear, and other are found. At $B_{\|}=10$ T, for example, the main difference is that the region of stability surrounded by the intersection of invariant tori differs significatively from Fig. 2(b) due to a shrinking along y direction. From comparison between Figs. 2 and 3 it is possible to observe that due to the distortion of the Fermi velocity of electrons along the x and y directions it also introduced an anisotropy of diffusion along transverse and longitudinal directions, which is manifested by a different electron dynamics.

In Fig. 4, we show typical periodic and quasiperiodic trajectories, calculated by means of the model for the electron dynamics in perpendicular magnetic field, for differet values of the ratio B/B_0 and a ratio of the antidot diameter, at the Fermi energy, to the artificial lattice period of $d/a=0.23$. These kind of orbits result from an isotropic Fermi velocity

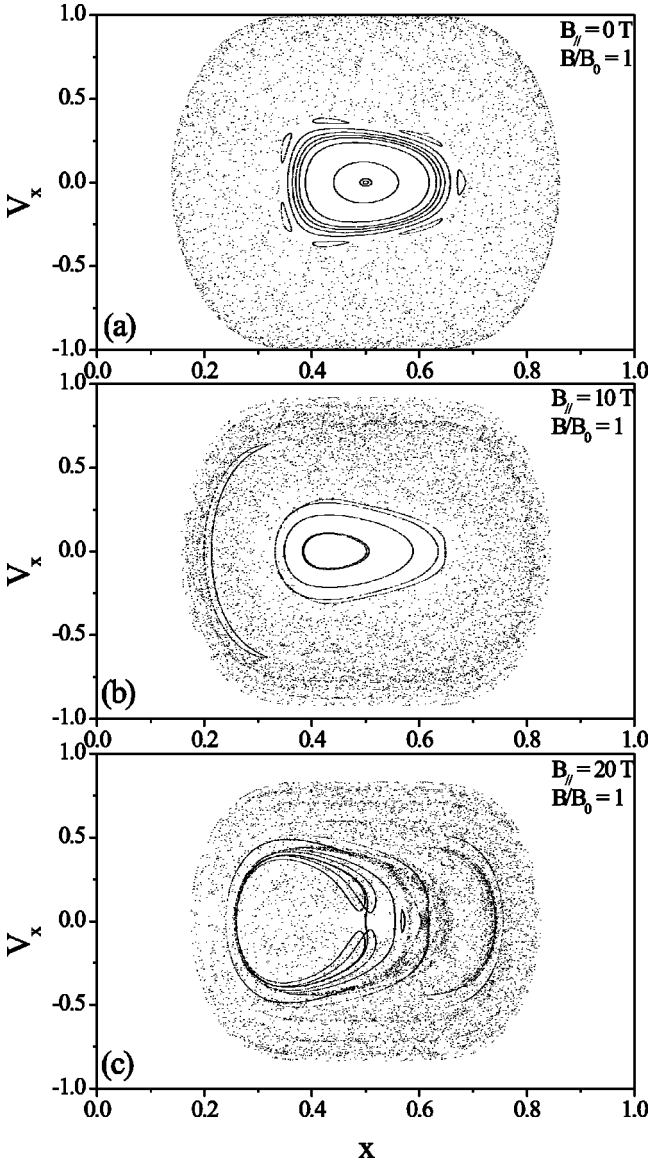

FIG. 2. Poincaré surfaces of the section in the rectangular antidot lattice at $y(\mathrm{mod}1)=0$ for $B/B_0=1$ and $d=0.23a$ for (a) $B_{\parallel}=0$ T, (b) $B_{\parallel}=10$ T, and $B_{\parallel}=20$ T.

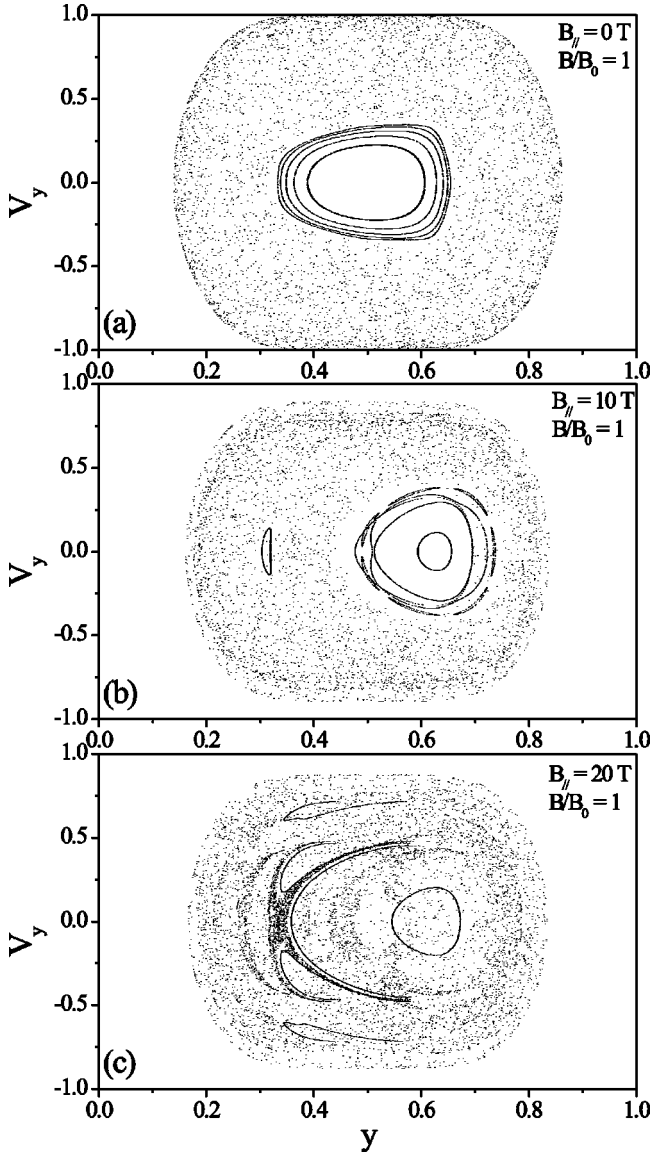

FIG. 3. Poincaré surfaces of the section in the rectangular antidot lattice at $x(\mathrm{mod}1)=0$ for $B/B_0=1$ and $d=0.23a$ for (a) $B_{\parallel}=0$ T, (b) $B_{\parallel}=10$ T, and $B_{\parallel}=20$ T.

along x and y directions. In order to compare, schematically, the evolution on the electron dynamics, in antidot lattice, subjected to in-plane magnetic field, Fig. 5 shows some regular electron trajectories resulting from the application of increasing parallel magnetic field on the 2DEG. Trajectories marked with numbers 1, 2, and 3 correspond to the condition $B/B_0=1$ and to a ratio $d=0.23a$. More specifically those orbits signed with 1 correspond to a parallel component $B_{\parallel}$ of 10 T, those marked with 2 correspond to $B_{\parallel}=20$ T, and trajectories with $B_{\parallel}=28$ T are signed by 3. Besides trapped orbits there are different kinds of ''run-away'' trajectories that evolve regularly between neighboring antidots increasing the diffusion along the longitudinal direction. This new kind of diffusive trajectories is only possible due to the asymmetric egglike shape of the Fermi contour.

B. Calculated magnetoresistance

Following the analytical models described above we also calculated the magnetoresistance for the 2DEG, in the presence of perpendicular magnetic field, and the behavior of such orbits with increasing in-plane magnetic field. Figure 6 depicts the results of the calculations. In Fig. 6(a) we show the normalized magnetoresistance ρ_{xx}/ρ_{xx0} as a function of the normalized magnetic field B/B_0. The first curve in the lower part corresponds to the application of perpendicular magnetic field $\Theta=90°$, and the next consecutive curves toward the upper part, correspond to the application of increasing parallel component of the field. All curves were shifted vertically in order to show clearly the evolution of the shift and broadening of the peaks together with the arising of the proposed structure. The calculations correspond, also to an antidot cross section at the Fermi energy, of $d=0.23a$ that is

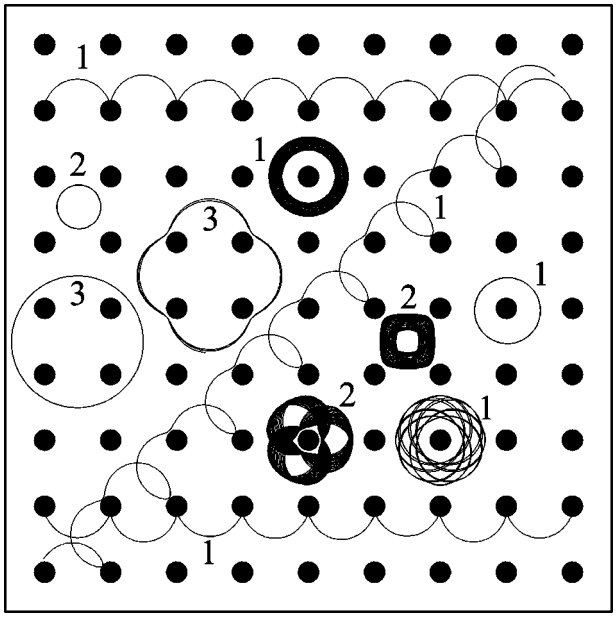

FIG. 4. Common electron trajectories, which develops in phase space in antidot lattice subjected to perpendicular magnetic field, (1) for $2R_c = a$, (2) $2R_c < a$, and (3) $2R_c > a$.

approximately the experimental situation of the sample with $a = 0.5$ μm. In Fig. 6(b) we show two calculated magnetoresistance curves for a cross section, at the Fermi energy, of $d = 0.1a$. This corresponds to the experimental situation of our designed sample with $a = 1.0$ μm. The lower curve corresponds to the application of perpendicular magnetic field and the other to the application of a parallel component of 28 T. From the calculations shown in Fig. 6 we have observed a broadening and a shift of the commensurability peaks. The anisotropy of the electron magnetic focusing effect[32] must be

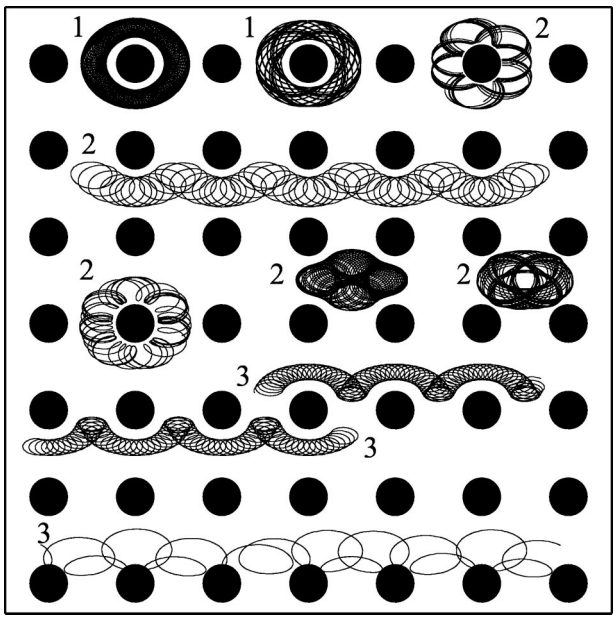

FIG. 5. Some regular trajectories, in tilted magnetic field, for $B/B_0 = 1$ and (1) $B_{\parallel} = 10$ T, (2) $B_{\parallel} = 20$ T, and (3) $B_{\parallel} = 28$ T.

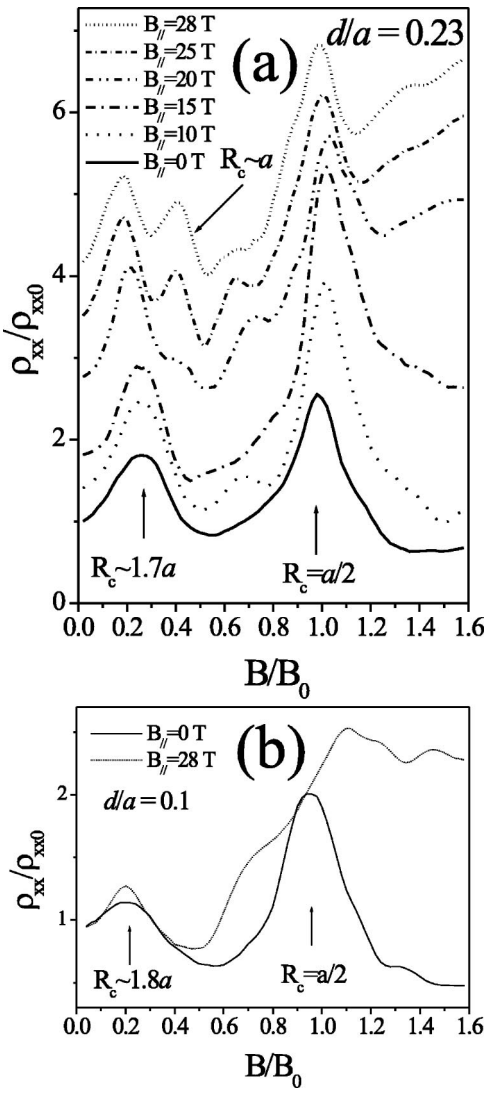

FIG. 6. (a) Calculated magnetoresistance ρ_{xx}/ρ_{xx0} for a 2DEG in antidot lattice with a ratio $d/a = 0.23$. We show the evolution of the commensurability peaks as a function of the increment of the in-plane component of the magnetic field. The curve at bottom (solid line) corresponds to the application of perpendicular field $\Theta = 90°$, and the uppermost curve corresponds to the application of a parallel component of $B_{\parallel} \sim 28$ T ($\Theta \sim 0.54°$). Curves for tilted field were shifted upward for a better view. (b) Calculated magnetoresistance in perpendicular and tilted magnetic field for a ratio $d/a = 0.1$.

responsible for this effect. The lattice separation between neighboring antidots, along either direction, acts like a injector/collector of electrons, the peaks on the resitivity result from the commensurability between the cyclotron diameter and the lattice constant a. As the in-plane component of the field is increased the matching condition is severely altered, in the x and y directions, as a consequence the degree of chaos in phase space is also increased and the peaks broaden and shift, and this phenomena increases as the ratio d/a diminishes. We have also analyzed, by means of Poincaré surface of the section, the effect of the arising of the additional commensurability peak. In order to compare we have calculated a surface of section at $[y(\mathrm{mod}1) = 0]$ for the

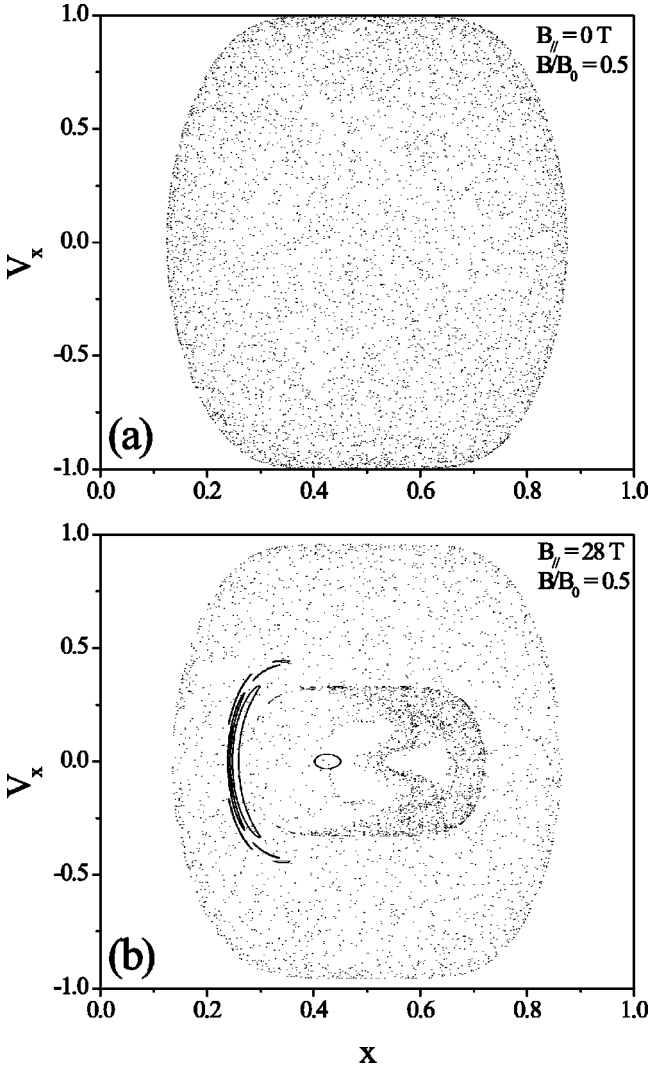

FIG. 7. Poincaré surfaces of sections in the rectangular antidot lattice at $y(\mathrm{mod}1)=0$ for $B/B_0=0.5$ and $d=0.23a$ for (a) $B_{\parallel}=0$ T, (b) $B_{\parallel}=28$ T.

same ratio $d=0.23a$ corresponding to our sample with lattice constant $a=0.5$ μm, this time for a normalized magnetic field $B/B_0=0.5$ that corresponds approximately to the commesurability condition $R_c=a$. The results are shown in Fig. 7, in the upper part (a) we have the surface of section for perpendicular magnetic field, and at bottom (b) we have the map for the case of the application of ~ 28 T parallel component of the magnetic field. For the case of perpendicular field most part of the surface of section corresponds to chaotic motion, this is in accord with calculations performed by Flieber *et al.*[7] for the phase-space volume of cyclotron trajectories with approximately similar ratio and commensurability condition $R_c=a$. There are also two islands of regular motion on the Poincaré surfaces of the section corresponding to trajectories trapped between four antidots that corresponds to a fixed point of hyperbolic type,[30] these kind of orbits are unstable under the application of a small electric field turning to chaotic or driftinglike trajectories. When a strong in-plane component of the magnetic field is applied the surface of the

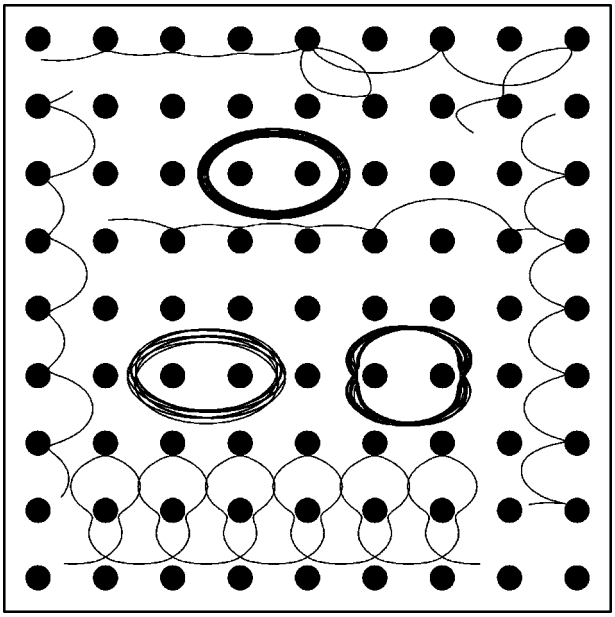

FIG. 8. Some regular trajectories, in tilted magnetic field, for $B/B_0=0.5$ and $B_{\parallel}=28$ T.

section at $[y(\mathrm{mod}1)=0]$ is strongly modified. As can be seen, in Fig. 7, a large fraction of phase space is now occupied by periodic and quasiperiodic orbits, also, there is an increment of drifting trajectories when compared with the Poincaré surface for perpendicular magnetic field, this type of orbits must be responsible for an enhancement of diffusion at low magnetic field and also for the arising of the additional peak. Also, we have several invariant tori but they correspond to trajectories that do not contribut to the conductivity, because they are pinned by the antidot and do not respond to a weak electric field.[11] Figure 8 shows a scheme of some regular trajectories, which develop, in phase space when $B/B_0=0.5$ and $B_{\parallel}=28$ T.

IV. EXPERIMENTAL RESULTS

A. Fabrication of samples and experimental technique

The four antidot samples were fabricated from a high-mobility $GaAs/Al_xGa_{1-x}As$ heterojunction. These heterostructures were grown by molecular-beam epitaxy with the following configuration: over a (100) semiinsulating GaAs substrate was deposited a 1.0 μm GaAs buffer layer, followed by 20 $AlAs_5GaAs_{10}$ periods (where 5 and 10 stand for the number of monolayers of each material), over this superlattice was grown an undoped 9000-ÅGaAs layer followed by 3 AlAs monolayers, 800 Å of a Si doped $Al_{0.3}Ga_{0.7}As$ layer, and finally a 100 Å of a Si doped GaAs layer. After growing, a 50-μm-wide Hall bar was patterned for each sample by means of conventional techniques, then, a rectangular array (100×50 μm), of circular-shaped artificial scatterers was superimposed over the poly(methyl methacrylate) (PMMA) layer of each bar through high-energy electron-beam lithography. The antidot lattice period a was chosen to be 0.5, 1.0, 1.5, and 2.0 μm for each sample. The

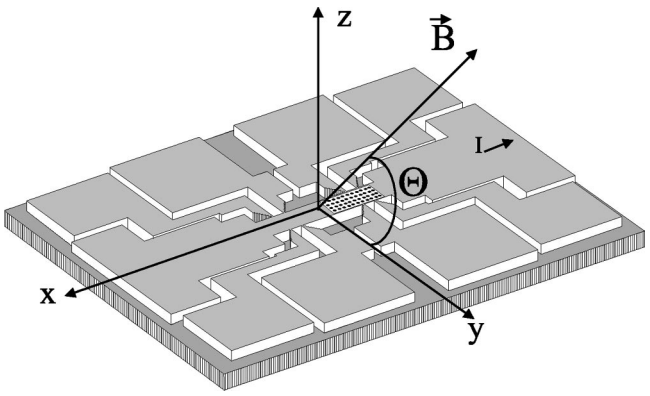

FIG. 9. Schematic view of a sample, containing an antidot lattice in a Hall bar. We show the configuration for tilted magnetic-field measurements. $\Theta = 90°$ corresponds to perpendicular configuration and $\Theta = 0°$ corresponds to the magnetic field parallel to the sample surface and also to the electric current.

antidot pattern was transferred across the GaAs/$Al_xGa_{1-x}As$ interface by plasma etching. The physical diameter of the antidots d_{lith} is approximately 0.1 μm. Before patterning the electron mobility μ_e, of the samples range between 0.610^6 and 1.010^6 $cm^2/V\,s$. For the application of high magnetic fields we used the European facility of the LCMI at CNRS in Grenoble. All measurements were performed at the temperature of 1.5 K, we employed lock-in technique for detection with an ac current not exceeding 10^{-6} A, the distance between potentiometric probes is 100 μm. Longitudinal and transversal resistance were simultaneously recorded for different angles between magnetic field and the substrate plane using an *in situ* system for rotation of the samples. We used Hall effect for the determination of the angle with a presicion of 0.05°.

B. Magnetoresistance measurements

In order to develop our experiment we first performed resistivity ρ_{xx} measurements, for each of the four samples, with the magnetic-field vector $\vec{B}$ applied perpendicularly to the plane of the 2DEG. Then, for each sample, we begin to rotate the sample, in steps, in order to increase the parallel component of the magnetic field along the surface of the sample, Fig. 9 shows a scheme of the sample with the angle of rotation (Θ). After each step of rotation a new resistivity measurement was done. As the perpendicular component of the magnetic field $B_\perp$ decreases we applied up to 28 T to record the evolution of the peaks when the samples were in almost parallel magnetic field. Figure 10 shows the magnetoresistance measurements, for the samples with periods $a = 1.0$ μm and $a = 0.5$ μm, taken at the temperature of 1.5 K, after a brief illumination, and as a function of the in-plane component of the magnetic field. For comparative reasons, we have normalized each magnetoresistance curve, first, with respect to the perpendicular component of the magnetic field $B\sin(\Theta)$, with the aid of the Hall resistance measurements ρ_{xy}, and second in relation to the resistivity in zero field. Θ

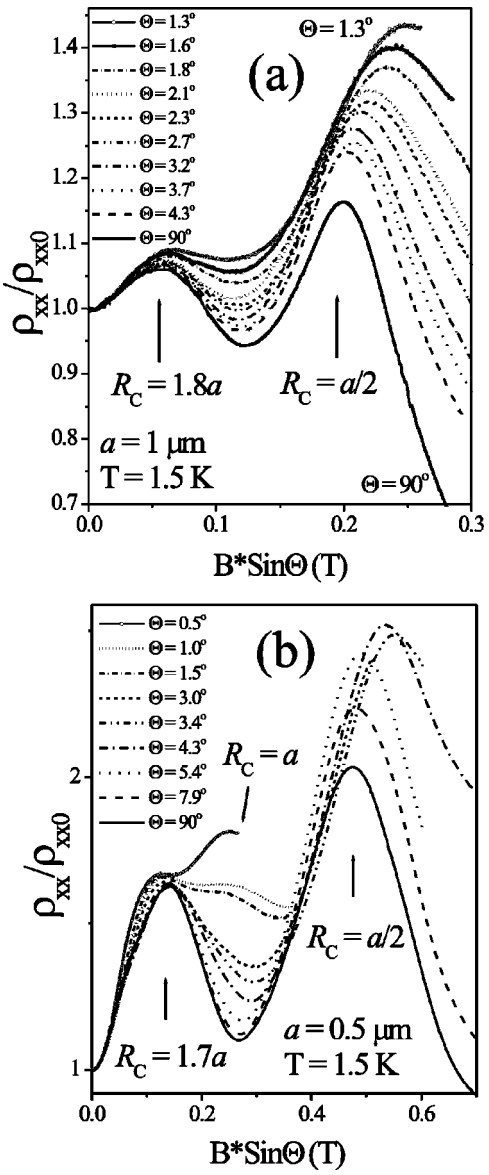

FIG. 10. Normalized experimental magnetoresistance data (ρ_{xx}/ρ_{xx0}) taken at the temperature of 1.5 K, for antidot lattice in 2DEG, as a function of the normalized perpendicular magnetic field (B/B_0), and also of the angle Θ. In (a) for the sample with $a = 1.0$ μm, and in (b) for $a = 0.5$ μm.

is the angle between the magnetic-field vector $\vec{B}$ and the surface of the sample. From Fig. 10 we can see that in perpendicular magnetic field ($\Theta = 90°$) we observe two pronounced commensurability peaks. The peak on the right, for each sample, correspond to the so-called condition $2R_c = a$ the other peak corresponds to $R_c \cong 1.8a$, for the sample with $a = 1.0$ μm, and $R_c \cong 1.7a$, for the sample with $a = 0.5$ μm. R_c stands for the classical cyclotron radius at the Fermi energy and is given by $R_c = \hbar\sqrt{2\pi N_s}/eB$. The two-dimensional Fermi energy, given by $E_F = (eBR_c)^2/2m^*$, is ≈ 12.0 meV and ≈ 16.6 meV for samples with $a = 1.0$ μm and $a = 0.5$ μm, respectively. Table I summarizes these data as well as the electron sheet density N_s and electron mobility μ_e, after patterning, for all samples.

TABLE I. Position of the commensurability peaks in perpendicular magnetic field (peak1 corresponds to $2R_c=a$), electron concentration, electron mobility, and 2D Fermi energy for each sample periodicity.

$a(\mu\text{m})$	0.5	1.0	1.5	2.0
Peak1(T)	0.48	0.20	0.13	0.10
Peak2(T)	0.14	0.05	0.06	0.05
Peak2(R_c/a)	1.70	1.80	1.20	1.17
$N_s(10^{11}\ \text{cm}^{-2})$	5.2	3.7	3.6	3.9
$\mu_e(10^5\ \text{cm}^2/\text{V s})$	4.4	3.6	2.9	4.0
E_F(meV)	16.6	12.0	11.5	12.5

As a first view it is possible to observe a strong broadening and also a shift of the main commensurability peak, for the case of the two samples, when the in-plane component of the magnetic field is steadily increased. It is also possible to observe, a more pronounced broadening, for the case of the sample with the larger period ($a=1.0\ \mu$m). Besides the effect of broadening and shifting of the peaks we can observe also, for the sample with $a=0.5\ \mu$m the arising of an additional commensurability peak that is located at a exact position corresponding to the commensurability condition $R_c=a$. Only the sample with the shortest period, and higher ratio d/a, showed this observed structure. This observation is in accordance with our calculations of ρ_{xx} in tilted magnetic field, and we attribute this phenomena to the enhancement of diffusion by the arising of regular trajectories at low magnetic field, as was shown from the analysis of the Poincaré surfaces of sections. These observed regular orbits do not exist in the presence of perpendicular magnetic field and become possible due to a steady change in the shape of the electron trajectories from circular to egglike because of the Fermi contour distortion in parallel magnetic field. The effect of shifting, of the commensurability peaks, can be explained by the elliptical shape of the electron trajectories, produced by the anisotropy of the Fermi contour in the x and y directions. This phenomenon can be seen as an increase or decrease of the electron effective mass (m_x^*, m_x^*), along these directions, as shown by calculations in Sec. III. Very recently a shift of commensurability peaks toward lower values of the perpendicular magnetic field was observed by Pogosov *et al.*[33] in antidots in 2DEG. They explained the effect by a change of the electron effective mass along y direction by the application of a strong parallel magnetic field. We also argue that the strong broadening of the commensurability peaks, which is observed for antidots with periods $a>1\ \mu$m, is explained, in an appropriate way, by an egglike Fermi contour. The egg shape of the Fermi contour produces electron trajectories with different shapes than those produced by an isotropic Fermi contour. As a consequence the magnetic focusing effect, which is mainly responsible for the regular circular orbits in antidot lattice,[25] is modified. Therefore these experiments give us information about the shape of the Fermi contour, which is not possible to obtain from the effective cyclotron mass measurements.[27] Figure 11 shows the comparison between the calculated and experimental shift of the main commensurability peak, relative to the position of the mean peak in perpendicular magnetic field, at $B_{\parallel}=28$ T as a function of the lattice period a and for each designed sample. The relative shifting shows an increasing behavior from 0.5 μm up to 1.5 μm where it reaches its maximum value and then falls rapidly for $a=2.0\ \mu$m. The shift of the peaks can be attributed to an increase of the diameter of the electron trajectories along the x direction, when the in-plane component of the magnetic field is increased. This effect changes steadily the commensurability condition $R_c/2=a$ to higher values of the magnetic field. As can be seen for Fig. 10 the relative shift increases for the sample with $a=1.5\ \mu$m and then it begins to decrease for shorter periods. As pointed out by Ando and co-workers,[34] for antidot lattices with large aspect ratio, the correlation between the electron motion before and after a collision with an antidot becomes more appreciable, so a larger aspect ratio corresponds to a small antidot period a and therefore to a narrow spacing between nearest-neighbor antidots, that could be the nature of the decreasing of the relative peak shift for shorter periods.

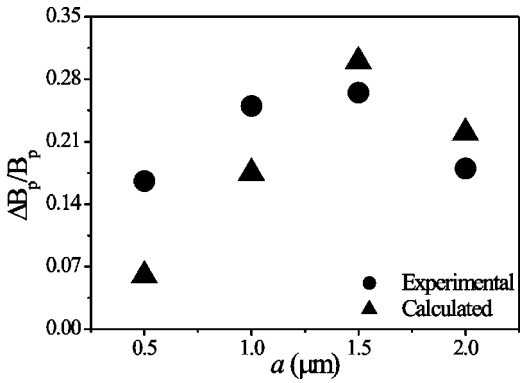

FIG. 11. Experimental (squares) and calculated (triangles) shift, in parallel field at 28 T, of the main commensurability peak relative to the peak position in perpendicular field, as a function of the antidot lattice period a.

V. SUMMARY

We have studied, through computational simulations and experimental measurements, the chaotic electron dynamics in arrays of antidots in patterned GaAs/Al_xGa_{1-x}As heterostructures, containing the 2DEG, when subjected to increasing in-plane magnetic field. From the analysis of the Poicaré surface of the sections and magnetoresistance calculations we attribute all these phenomena to the Fermi contour distortion induced by the high in-plane magnetic field.

ACKNOWLEDGMENTS

This work was supported by FAPESP and CNPQ Brazilian Funding Agencies. We would like to thank LCCA-USP by the computational facilities which made possible part of this work.

[1] K. Ensslin and P.M. Petroff, Phys. Rev. B **41**, 12 307 (1990).
[2] H. Fang and P.J. Stiles, Phys. Rev. B **41**, 10 171 (1990).
[3] D. Weiss, M.L. Roukes, A. Menschig, P. Grambow, K. von Klitzing, and G. Weimann, Phys. Rev. Lett. **66**, 2790 (1991).
[4] G.M. Gusev, Z.D. Kvon, L.V. Litvin, Yu.V. Nastaushev, A.K. Kalagin, and A.I. Toropov, J. Phys.: Condens. Matter **4**, L269 (1992).
[5] J. Wagenhuber, T. Geisel, P. Niebauer, and G. Obermair, Phys. Rev. B **45**, 4372 (1992).
[6] Dieter Weiss, Gerd Lutjering, and Klaus Richter, Chaos, Solitons Fractals **8**, 1337 (1997).
[7] M. Flieber, G.J.O. Schmidt, and H. Spohm, Phys. Rev. E **53**, 5690 (1996).
[8] Axel Lorke, J.P. Kotthaus, and Klaus Ploog, Phys. Rev. B **44**, 3447 (1991).
[9] G.M. Gusev, P. Basmaji, D.I. Lubyshev, L.V. Litvin, Yu.V. Nastaushev, and V.V. Preobrazhenskii, Phys. Rev. B **47**, 9928 (1993).
[10] G.M. Gusev, P. Basmaji, Z.D. Kvon, L.V. Litvin, Yu.V. Nastaushev, and A.I. Toropov, J. Phys.: Condens. Matter **6**, 73 (1994).
[11] Wenchang Lu, Phys. Rev. B **54**, 8049 (1996).
[12] E.M. Baskin, G.M. Gusev, Z.D. Kvon, A.G. Pogosov, and M.V. Entin, Pis'ma Zh. Eksp. Teor. Fiz. **55**, 649 (1992) [JETP Lett. **55**, 678 (1992)].
[13] Takashi Azuma and Toshihito Osada, Physica B **256**, 397 (1998).
[14] J. Eroms, M. Zitzlsperger, D. Weiss, J.H. Smet, C. Albrecht, R. Fleischmann, M. Behet, J. De Boeck, and G. Borghs, Physica B **256**, 409 (1998).
[15] R. Fleischmann, T. Geisel, and R. Ketzmerick, Phys. Rev. Lett. **68**, 1367 (1992).
[16] H. Silberbauer and U. Rössler, Phys. Rev. B **50**, 11 911 (1994).
[17] R. Schuster, G. Ernst, K. Ensslin, M. Entin, M. Holland, G. Böhm, and W. Klein, Phys. Rev. B **50**, 8090 (1994).
[18] K. Tsukagoshi, T. Nagao, M. Haraguchi, S. Takaoka, K. Murase, and K. Gamo, Superlattices Microstruct. **23**, 493 (1998).
[19] X. Kleber, G.M. Gusev, U. Gennser, D.K. Maude, J.C. Portal, D.I. Lubyshev, P. Basmaji, M.de P.A. Silva, J.C. Rossi, and Y.V. Nastaushev, Phys. Rev. B **54**, 13 859 (1996).
[20] S. de Haan, A. Lorke, R. Hennig, M. Suhrke, W. Wegscheider, and M. Bichler, Phys. Rev. B **60**, 8845 (1999).
[21] T. Jungwirth and L. Smrčka, J. Phys.: Condens. Matter **15**, L217 (1993).
[22] L. Smrčka and T. Jungwirth, J. Phys.: Condens. Matter **6**, 55 (1994).
[23] R.J. Warburton, M. Watts, R.J. Nicholas, J.J. Harris, and C.T. Foxon, Semicond. Sci. Technol. **7**, 787 (1992).
[24] W. de Lange, F.A.P. Blom, and J.H. Wolter, Semicond. Sci. Technol. **8**, 341 (1993).
[25] K. Ohtsuka, S. Takaoka, K. Oto, K. Murase, and K. Gamo, Physica B **249**, 780 (1998).
[26] J.M. Heisz and E. Zaremba, Semicond. Sci. Technol. **8**, 575 (1993).
[27] L. Smrčka, P. Vašek, J. Koláček, T. Jungwirth, and M. Curk, Surf. Sci. **361**, 509 (1996).
[28] U. Merkt, Phys. Rev. B **32**, 6699 (1985).
[29] R. Kubo, M. Toda, and N. Hashitsime, *Statistical Physics II* (Springer-Verlag, Berlin, 1985).
[30] M.V. Berry, in *Topics in Nonlinear Dynamics*, edited by S. Jorna, AIP Conf. Proc. 46 (American Institute of Physics, New York, 1978).
[31] T. Geisel, A. Zacherl, and G. Radons, Phys. Rev. Lett. **59**, 2503 (1987).
[32] H. van Houten, C.W.J. Beenakker, J.G. Williamson, M.E.I. Broekaart, P.H.M. van Loosdrecht, B.J. van Wees, J.E. Mooij, C.T. Foxon, and J.J. Harris, Phys. Rev. B **39**, 8556 (1989).
[33] A.G. Pogosov, M.V. Budantsev, A. Pouydebasque, M.V. Entin, D.K. Maude, J.C. Portal, A.E. Plotnikov, A.I. Toropov, and A.K. Bakarov, Physica B **298**, 291 (2001).
[34] Tsuneya Ando, Seiri Uryu, Satoshi Ishizaka, and Takeshi Nakanishi, Chaos, Solitons Fractals **8**, 1057 (1997).